Inorg. Chem. **2004**, *43*, 2189–2196

Investigation of Hydrothermal Routes to Mixed-Metal Cerium Titanium Oxides and Metal Oxidation State Assignment Using XANES

Christopher S. Wright,[†] Richard I. Walton,*[,†] David Thompsett,[‡] and Janet Fisher[‡]

Department of Chemistry, School of Biological and Chemical Sciences, University of Exeter, Stocker Road, Exeter EX4 4QD, U.K., and Johnson Matthey Technology Centre, Sonning Common, Reading, RG4 9NH, U.K.

Received October 22, 2003

The reaction between TiF_3 or TiO_2 and Ce^{3+} in sodium hydroxide solutions yields highly crystalline $NaCeTi_2O_6$ at room temperature and under mild hydrothermal conditions ($T \leq 240$ °C). There is no evidence for the formation of ternary Ce–Ti–O materials by this method, and the use of bases other than NaOH always produces poorly crystalline materials. The material $NaCeTi_2O_6$ has a distorted perovskite structure with sodium and cerium ions randomly occupying the A sites: *Pnma*, $a = 5.4517(8)$ Å, $b = 7.7292(6)$ Å, $c = 5.4573(3)$ Å. XANES spectroscopy at the Ti K edge and Ce L_{III} edge, with reference to crystalline model compounds, reveals that cerium is found solely as Ce(III) and titanium as Ti(IV) in $NaCeTi_2O_6$. Isomorphous substitution of Ce^{3+} by Nd^{3+} or Ti^{4+} by V^{4+} is found to be very facile under hydrothermal conditions (at a temperature of 240 °C), by addition of appropriate amounts of metal salts to the hydrothermal reaction mixtures. The series $NaCe_{1-x}Nd_xTi_2O_6$ ($0 \leq x \leq 1$) and $NaCeTi_{2-x}V_xO_6$ ($0 \leq x \leq 1.8$) can be formed directly in one step, and all materials were characterized by powder X-ray diffraction. The oxidation states of the substituent elements were determined using XANES spectroscopy, which further demonstrates that isomorphous substitution has taken place, with all vanadium present as V(IV) when the B site is substituted. Scanning electron microscopy analysis of the solids shows them to be made up of irregularly shaped particles made up of clusters of submicron-sized crystallites but that on firing in excess of 1000 °C the particle size is increased to ~10 μm and the particles have distinct, sharp edges.

Introduction

Low-temperature routes to mixed-metal oxides have attracted a great deal of interest for a number of years now.[1−4] The traditional high-temperature, ceramic method of solid-state chemistry in many cases allows the production of highly crystalline materials in a stoichiometric reaction, but it is lengthy (repeated cycles of grinding and heating of solid reactants are necessary) and offers no control over particle size and morphology, which would be highly desirable in the optimization of physical properties of a material for practical application. Furthermore, since the temperatures used in the ceramic method are high (in excess of 1000 °C), there is little scope for the preparation of metastable, kinetic phases which themselves might have interesting properties. One of the best known "*chimie douce*" methods for the preparation of mixed-metal oxides is the sol−gel technique: this permits intimate mixing of the constituent elements prior to firing, by the precipitation of an amorphous gel phase, and so the temperature utilized in the production of the material is lowered (although it is still typically in excess of 600 °C if highly crystalline materials are required).[3] The hydrothermal method, usually used for the synthesis of zeolites and other microporous solids, has been used with some success in the synthesis of ternary and more complex transition metal oxides in recent years,[5,6] although the method has not yet been extensively explored for the preparation of such materials. Subcritical conditions are often used in hydrothermal synthesis, typically temperatures of less than 250 °C, and the use of a sealed autoclave produces mild,

* Author to whom correspondence should be addressed. E-mail: r.i.walton@exeter.ac.uk.
[†] University of Exeter.
[‡] Johnson Matthey Technology Centre.

(1) Rouxel, J.; Tournoux, M.; Brec, R. *Soft Chemistry Routes to New Materials*; Trans Tech Publications: Uetikon-Zuerich, Switzerland, 1994.
(2) Rouxel, J.; Tournoux, M. *Solid State Ionics* **1996**, *84*, 141.
(3) Gopalakrishnan, J. *Chem. Mater.* **1985**, *7*, 1265.
(4) Rao, C. N. R.; Gopalakrishnan, J. *New Directions in Solid State Chemistry*; Cambridge University Press: Cambridge, 1997.
(5) Demazeau, G. *J. Mater. Chem.* **1999**, *9*, 15.
(6) Walton, R. I. *Chem. Soc. Rev.* **2002**, *31*, 230.

10.1021/ic035211u CCC: $27.50
Published on Web 02/26/2004

autogenous pressures (around 20 atm). In certain cases, these conditions can also allow the direct formation of solids usually prepared via the ceramic route: for example, barium titanate, $BaTiO_3$, forms at temperatures as low as 80 °C from alkali solutions of barium salts and the anatase polymorph of TiO_2.[7−9] More complex systems can also be produced in one step (without the need for annealing); for example, we have recently shown that the manganites $Ln_{1-x}A_xMnO_3$ (Ln = La, Pr and A = Ba, Sr, Ca) can be produced at 240 °C in 24 h in a hydrothermal autoclave.[10]

Aside from barium titanate, whose hydrothermal synthesis has been particularly well studied because of the uses of the solid in various electronic devices, the hydrothermal synthesis of a number of titanates has recently been described. For example, the hydrothermal synthesis of lead zirconate titanate has been utilized to prepare thin films of the solid,[11,12] Du et al. have recently described the hydrothermal formation of potassium titanate nanowires,[13] the hydrothermal formation of nanotubes of titanate perovskites has been reported,[14] and, in a particularly interesting study of the hydrothermal formation of $Na_{0.5}Bi_{0.5}TiO_3$, Lencka et al. calculated "stability and yield" diagrams to plot the effect of reaction conditions on the outcome of reaction, allowing the conditions required for the isolation of pure product to be identified easily.[15] To the best of our knowledge, the hydrothermal synthesis of cerium titanates has not been investigated. These materials are interesting to study because of the possibility of variability of oxidation state of both cerium and titanium; indeed, by conventional ceramic routes, materials with a variety of combinations of oxidation states can be produced.[16] These include solids containing Ce^{IV}/Ti^{IV} such as $CeTi_2O_6$,[17] Ce^{III}/Ti^{IV}, such as Ce_2TiO_5, $Ce_2Ti_2O_7$, and $Ce_4Ti_9O_{24}$,[18] and in the lanthanide-deficient perovskite $Ce_{2/3}TiO_3$,[19] $Ce^{III}/Ti^{III}/Ti^{IV}$, for example, the series $Ce_2O_3{\cdot}nTiO_{2-m}$,[16] and Ce^{III}/Ti^{III} as seen in the perovskite $CeTiO_3$.[20] More complex systems have also been studied; for example, in the series $Ce_{1-x}A_xTiO_3$ (A = Sr, Ba), substitution of cerium (III) by an alkaline earth metal results in oxidation of titanium(III) to titanium (IV).[21] It is interesting to note that for many materials in the cerium titanate system, direct measurement of the metal oxidation states has never been undertaken, and instead has been inferred from the reaction conditions and starting materials needed in synthesis. For example, in the preparation of $Ce_2Ti_2O_7$, a redox reaction between the reagents CeO_2 and Ti_2O_3 is assumed to result in the formation of the Ce^{III}/Ti^{IV} oxide.[18]

Ceria−titania composites have found some use as catalysts, developed because of the considerable applications of ceria-based catalysts in automobile exhaust treatment. For example, Reddy et al. have recently described CeO_2–TiO_2 redox catalysts prepared by hydrolysis and coprecipitation from $CeCl_3$ and $TiCl_4$ solutions,[22] whereas similar oxidation catalysts reported by Rynkowski et al. contained a number of unidentified mixed-metal oxides.[23] In ceria catalysts, the interconversion of the Ce^{III} and Ce^{IV} oxidation states is the key to their activity, and thus it is important to study new synthetic routes to cerium oxides that might provide access to unusual mixtures of oxidation states. Herein we report an investigation of the hydrothermal synthesis of cerium titanium oxides and related phases produced by inclusion of other rare earths, or other transition metals, and use XANES spectroscopy to assign oxidation states of constituent metals.

Experimental Section

Materials Synthesis. Hydrothermal syntheses were performed using 25 mL Teflon-lined stainless steel autoclaves. The reagents were all metal salts purchased from chemical companies: $CeCl_3{\cdot}7H_2O$ (Avocado), TiO_2, TiF_3 (Aldrich), VCl_3 (Fisher), and $NdCl_3{\cdot}6H_2O$ (Aldrich). The approximate amount of water in the salts was determined by gravimetric analysis. Reactions were performed at temperatures between 100 and 240 °C after stirring the reagents in basic solution for around 30 min (see below for discussion of the bases used). After cooling, solids were recovered by suction filtration, washed thoroughly with distilled water, and dried in air at 50 °C. Several crystalline model compounds were used in the XANES studies: these were purchased from chemical companies, and their identities were confirmed by powder X-ray diffraction. $NaTi_2O_4$ was kindly synthesized and donated by Professor M. J. Geselbracht of Reed College, Oregon.

Laboratory Characterization. Powder X-ray diffraction (PXRD) data were recorded on a Bruker D8 diffractometer operating with Cu Kα (average $\lambda = 1.5418$ Å). Data were typically measured using a step size of $0.02°2\theta$, with a counting time of 2 s. Data were analyzed using the programs Celref[24] and Fullprof,[25] which allowed refinement of cell parameters and calculation of powder patterns from a structural model, respectively. Scanning electron microscopy studies were performed using a Leica S440i microscope fitted with an Oxford Instruments ISIS EDX analytical system. Powdered samples were placed onto a carbon tab and a carbon coat was applied. An accelerating voltage of 10 kV and probe current of 5000 pA was used for analysis. XPS analysis was performed using

(7) Dutta, P. K.; Gregg, J. R. *Chem. Mater.* **1992**, *4*, 843.
(8) Clark, I. J.; Takeuchi, T.; Ohtori, N.; Sinclair, D. C. *J. Mater. Chem.* **1999**, *9*, 83.
(9) Walton, R. I.; Millange, F.; Smith, R. I.; Hansen, T.; O'Hare, D. *J. Am. Chem. Soc.* **2001**, *123*, 12547.
(10) Spooren, J.; Rumplecker, A.; Millange, F.; Walton, R. I. *Chem. Mater.* **2003**, *15*, 1401.
(11) Zeng, J. M.; Lin, C. L.; Song, Z. T.; Li, K.; Li, J. H. *Philos. Mag. Lett.* **2000**, *80*, 119.
(12) Su, B.; Ponton, C. B.; Button, T. W. *J. Eur. Ceram. Soc.* **2001**, *21*, 1539.
(13) Du, G. H.; Chen, Q.; Han, P. D.; Yu, Y.; Peng, L. M. *Phys. Rev. B* **2003**, *67*, 035323.
(14) Mao, Y. N.; Banerjee, S.; Wong, S. S. *Chem. Commun.* **2003**, 408.
(15) Lencka, M. M.; Oledzka, M.; Riman, R. E. *Chem. Mater.* **2000**, *12*, 1323.
(16) Bamberger, C. E.; Haverlock, T. J.; Shoup, S. S.; Kopp, O. C.; Stump, N. A. *J. Alloys Compd.* **1994**, *204*, 101.
(17) Bazuev, G. V.; Makarov, O. V.; Zhilyaev, V. A.; Shveikin, G. P. *Russ. J. Inorg. Chem.* **1976**, *23*, 1447.
(18) Preuss, A.; Gruehn, R. *J. Solid State Chem.* **1994**, *110*, 363.
(19) Yoshii, K. *J. Alloys Compd.* **2000**, *305*, 72.
(20) Maclean, D. A.; Greedon, J. E. *Inorg. Chem.* **1981**, *20*, 1025.
(21) Sunstrom, J. E.; Kauzlarich, S. M.; Antonio, M. R. *Chem. Mater.* **1993**, *5*, 182.
(22) Reddy, B. M.; Khan, A.; Yamada, Y.; Kobayashi, T.; Loridant, S.; Volta, J.-C. *J. Phys. Chem. B* **2003**, *107*, 5162.
(23) Rynkowski, J.; Farbotko, J.; Touroude, R.; Hilaire, L. *Appl. Catal. A* **2000**, *203*, 335.
(24) Laugier, J.; Bochu, B. *Celref*; http://www.inpg.fr/LMGP; Laboratoire des Materiaux et du Génie Physique de l'Ecole Supérieure de Physique de Grenoble.
(25) Rodriguez-Carvajal, J. In *Collected Abstracts of Powder Diffraction Meeting*; Toulouse, 1990; p 127.

Table 1. Reaction Conditions Investigated for the Hydrothermal Preparation of Cerium Titanate Materials[a]

chemicals[b]	temp (°C)	time (h)	solid product(s)
$CeCl_3{\cdot}7H_2O{:}TiO_2{:}16NaOH{:}440H_2O$	240	24	$NaCeTi_2O_6 + CeO_2$
$CeCl_3{\cdot}7H_2O{:}TiO_2{:}440H_2O$	240	24	CeO_2 (poorly crystalline) + TiO_2
$CeCl_3{\cdot}7H_2O{:}2.5TiO_2{:}40NaOH{:}550H_2O$	240	24	$NaCeTi_2O_6 + CeO_2$ (trace)
$CeCl_3{\cdot}7H_2O{:}2.5TiF_3{:}40NaOH{:}550H_2O$	240	24	$NaCeTi_2O_6$
$CeCl_3{\cdot}7H_2O{:}2.5TiF_3{:}40NaOH{:}550H_2O$	25	1	$NaCeTi_2O_6$
$CeCl_3{\cdot}7H_2O{:}1.25TiF_3{:}1.25TiO_2{:}40NaOH{:}550H_2O$	240	24	$NaCeTi_2O_6$
$CeCl_3{\cdot}7H_2O{:}2.5TiF_3{:}68KOH{:}550H_2O$	240	24	$CeF_3 + TiO_2$
$CeCl_3{\cdot}7H_2O{:}2.5TiF_3{:}68Me_4NOH{:}550H_2O$	240	24	$CeF_3 + TiO_2$
$(1-x)CeCl_3{\cdot}7H_2O{:}xNdCl_3{:}2.5TiF_3{:}40NaOH{:}550H_2O$	240	24	$NaCe_{1-x}Nd_xTi_2O_6$ $(0 \le x \le 1)$
$CeCl_3{\cdot}7H_2O{:}(2.5-x)TiF_3{:}xVCl_3{:}40NaOH{:}550H_2O$	240	24	$NaCeTi_{2-x}V_xO_6$ $(0 \le x \le 1.8)$
$CeCl_3{\cdot}7H_2O{:}2.5VCl_3{:}40NaOH{:}550H_2O$	240	24	$CeO_2 + Ce(OH)_3 + VO_2$

[a] See text for discussion of product identification. [b] Typically 0.4 g of $CeCl_3$ was utilized, and 10 mL of water, giving autoclave percentage fill of ~40−50%.

a Thermo VG ESCALAB 250 instrument. The samples were mounted using double-sided adhesive tape and analyzed using monochromatic Al Kα radiation at 150 W and a 500 μm spot. Scans were carried out with a 40 eV pass energy using the Ti 2p emission at 458.3 eV and the C 1s emission at 284.8 eV as references. ICP analysis for metals was performed at the Johnson Matthey Technology Centre.

X-ray Absorption Studies. XANES (X-ray absorption near-edge structure) experiments were performed on Station 7.1 of the Daresbury Synchrotron Radiation Source (SRS) at the titanium K edge (~4966 eV), vanadium K edge (~5465 eV), and cerium L_{III} edge (~5723 eV). The SRS operates with an average stored energy of 2 GeV and a typical electron current of 200 mA, and Station 7.1 receives X-rays in the 4−10 keV energy range. The station is equipped with a harmonic-rejecting, double-crystal Si(111) monochromator, the second crystal of which allows sagittal focusing of the X-ray beam. Harmonic rejection was set to 50% for all experiments, by detuning the second crystal to 50% of the maximum X-ray intensity. Data were collected in transmission mode from pellets prepared by pressing powdered sample materials diluted, when necessary, with polyethylene powder (spectrophotometric grade, Aldrich). Dilution was required to prevent self-absorption (values for the full absorption and edge jump of $\mu d \approx 2.5$ and $\Delta\mu d \approx 1$ are used). Ionization chambers placed before (I_0) and behind (I_t) the sample were filled with appropriate quantities of inert gases (Ar−He mixture) to maximize the detection of the X-rays. Data were also measured simultaneously from a 5 μm metal foil placed between the second and a third ionization chamber (I_m) to provide an edge-shift calibration for the XANES data. Data were collected in two regions: (1) the preedge region with a step size equivalent to 10 eV to allow a preedge background calculation and subtraction; (2) the XANES (X-ray absorption near-edge structure) region from 30 eV below the edge to 50 eV above the absorption edge, with a step size equivalent to ~0.2 eV. The data were analyzed using the Daresbury Laboratory suite of software.[23] The program EXCALIB was used to normalize all data. EXBROOK was used to produce normalized XANES spectra by the edge step method and by positioning the E_0 value using the maximum in the first derivative, recalibrating the spectrum around this value, and then subtracting the preedge background using a quadratic fit.

Results and Discussion

$NaCeTi_2O_6$. Our initial studies focused upon the hydrothermal reaction between various cerium and titanium salts or oxides in basic, aqueous solution. We chose high pH conditions since the majority of hydrothermal synthesis of mixed-metal oxides have been reported to take place under such conditions.[6] The reaction between $CeCl_3{\cdot}nH_2O$ ($n = 6.9$) and TiF_3 was found to produce phase-pure samples of a pale brown solid, which we subsequently show to be $NaCeTi_2O_6$ (see below). Table 1 summarizes the outcome of typical reactions, carried out with a variety of starting materials and reaction conditions. We found that an excess of titanium is always necessary to produce the desired product; the extra titanium remains in solution, which was detected by ICP analysis of the filtrate. Interestingly, in contrast, for the hydrothermal synthesis of barium titanate, an excess of Ba^{2+} is required to achieve complete conversion to $BaTiO_3$.[7,8] $NaCeTi_2O_6$ is also produced if TiO_2 (anatase polymorph) is used as the titanium source, although in this case a small amount of CeO_2 is often present as an impurity, suggesting again that excess titanium remains in solution. Reactions using bases other than sodium hydroxide never produced any cerium titanium oxides: if KOH was used, the solid always consisted of poorly crystalline material, the sharpest diffraction features being consistent with the presence of the anatase polymorph of TiO_2; if alkylammonium hydroxides were used, only CeF_3 and TiO_2 were produced and in the case of calcium hydroxide the major component of the product was recrystallized $Ca(OH)_2$. This indicated that the presence of sodium was necessary for the formation of the cerium titanate crystalline product. Verification of the presence of sodium in the product was obtained by XPS measurements which showed a distinct Na 1s emission, and also EDXA analysis on the SEM, which showed Na K X-ray fluorescence from every region of sample analyzed. ICP analysis confirmed the bulk chemical composition of the solid as $NaCeTi_2O_6$: found, 40.9% Ce and 24.1% Ti; expected, 39.5% Ce and 27.0% Ti.

Powder X-ray diffraction reveals that hydrothermal $NaCeTi_2O_6$ is isostructural with "synthetic loparite" reported by Chakhmouradian et al.[26] Figure 1 shows laboratory powder XRD data from our hydrothermal sample and the pattern calculated for synthetic loparite (using the cell parameters refined from our data: orthorhomic *Pnma*, $a = 5.4517(8)$ Å, $b = 7.7292(6)$ Å, $c = 5.4573(3)$ Å). Loparite is a mineral with typical composition (Ln,Na,Sr,Ca)(Ti,Nb,Ta,Fe)$_2O_3$ [Ln = lanthanide], and has been an

(26) Chakhmouradian, A. R.; Mitchell, R. H.; Pankov, A. V.; Chukanov, N. V. *Mineral. Mag.* **1999**, *63*, 519.

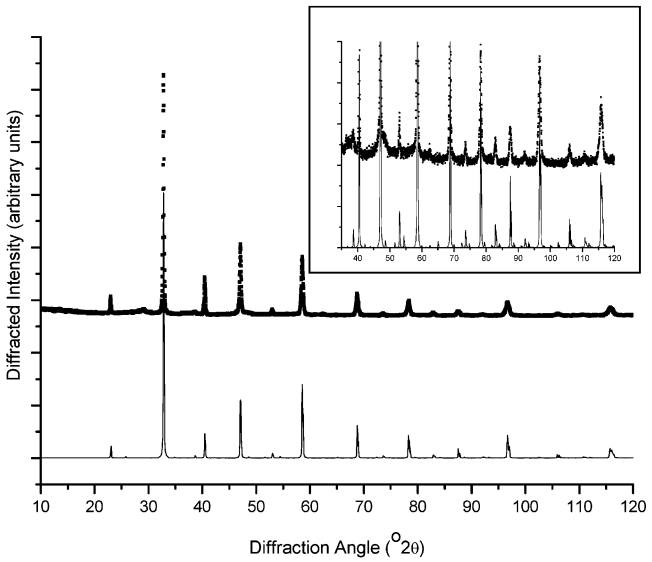

Figure 1. Powder X-ray diffraction data of hydrothermal $NaCeTi_2O_6$. Points are experimental data, and the full line is the pattern calculated from the structural model based on that for natural loparite by Chakhmouradian et al.:[26] orthorhomic *Pnma*, $a = 5.4566(3)$ Å, $b = 7.7279(5)$ Å, $c = 5.4586(8)$ Å. The inset shows the high angle region of the data. The broad peak at $\sim 27°2\theta$ is due to a trace amount of CeO_2 impurity.

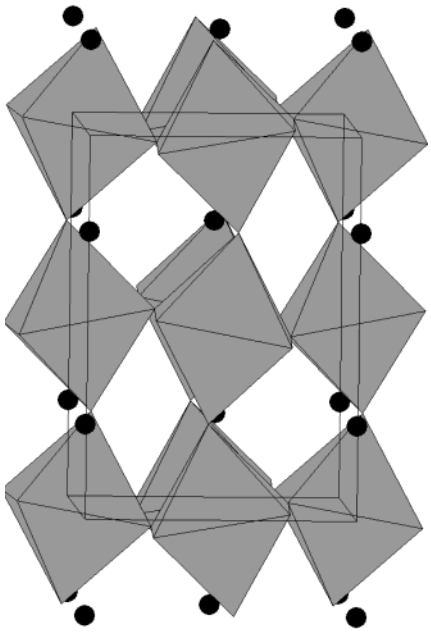

Figure 2. Polyhedral view of the structure of $NaCeTi_2O_6$. Shaded octahedra are $\{TiO_6\}$ units, and the circles are Na/Ce sites.

important source of lighter rare earth metals in Russia.[27] In recent years, natural samples of loparite have been the focus of structural investigation,[28] and as part of this survey Chakhmouradian et al. synthesized a synthetic analogue for comparison.[26] This was achieved using a high-temperature route from CeO_2 and TiO_2 accomplished in the presence of charcoal as a reducing agent at 1000 °C. The material prepared by that method contained significant amounts of crystalline TiO_2 and CeO_2 as byproducts. Our new hydrothermal synthesis route is a much more straightforward means to prepare highly crystalline pure samples of the material. (It should be noted that all of our powder XRD data are from samples isolated from the reaction solutions without any postsynthesis annealing.) Loparite has a distorted perovskite-type structure with Ce^{3+} and Na^+ ions randomly occupying the A-site positions, as shown in Figure 2. The tolerance factor calculated using standard ionic radii[29] is 0.85, consistent with the $GdFeO_3$-type distortion of the perovskite structure.

The oxidation states of cerium and titanium in $NaCeTi_2O_6$ have never been directly measured. It has instead been assumed that the material contains solely Ce^{III} and Ti^{IV}, based upon the assumption that the charcoal used in its ceramic synthesis acted as a reducing agent for the CeO_2 starting material.[26] Since we can prepare our material most effectively from Ce^{III} and Ti^{III}, and traces of CeO_2 are occasionally seen as a byproduct, we had to rule out possible formulations of loparite that contain Ce^{IV} and Ti^{III}, such as $NaCe^{IV}Ti^{III}Ti^{IV}O_6$. Bond valence sums[29] give the valence for Ti as 4.22, and for Ce as 2.90, but we wished to measure independent, complementary data to confirm the oxidation states of the metal. XPS spectra (see Supporting Information) in the cerium 3d region are typical of cerium(III) oxides, and are rather different from CeO_2; in particular the peaks at 885 and 908 eV are characteristic of Ce(III).[30,31] The titanium 2p region shows a strong peak at 458.3 eV, which may be due to either Ti(III) or Ti(IV). The difference in binding energy between the two oxidation states is small, making it difficult to detect mixtures of the two oxidation states,[32] and this is further complicated by the fact that the XPS method is sensitive to the surface of the sample rather than the bulk. To provide further, and unambiguous, evidence for the oxidation state of the metals in our materials, we turned to XANES spectroscopy, since it is well-known that the spectral features of the near-edge region of the X-ray absorption spectra are affected by the oxidation state of the element studied, and that the method provides a qualitative fingerprint of electronic structure and local atomic environment. One other important advantage of XANES spectroscopy is that it is element specific. Figure 3 shows the titanium XANES data of our sample of loparite and of materials that contain titanium in three different oxidation states. It can be seen that the edge position lies at lower energy for the spectra from compounds with lower titanium oxidation state (the edge position quoted here is the energy for which normalized absorption equals 0.5). This has previously been reported in the literature;[33,34] for example, Durmeyer showed the edge position to drop by ~ 2 eV between TiO_2 and $LiTi_2O_4$.[33] The

(27) Hedrick, J. B.; Sinha, S. P.; Kostnkin, V. D. *J. Alloys Compd.* **1997**, *250*, 467.
(28) Mitchell, R. H.; Burns, P. C.; Chakhmouradian, A. R. *Can. Mineral.* **2000**, *38*, 145.
(29) Brown, I. D.; Altermatt, D. *Acta Crystallogr., Sect. B* **1985**, *41*, 244.
(30) Mullins, D. R.; Overbury, S. H.; Huntley, D. R. *Surf. Sci.* **1998**, *409*, 307.
(31) Nédélec, J.-M.; Gengembre, L.; Turrell, S.; Bouazaoui, M.; Grimblot, J. *Appl. Surf. Sci.* **1999**, *142*, 243.
(32) Mayer, J. T.; Diebald, U.; Madley, T. E.; Garfunkel, E. *J. Electron Spectrosc. Relat. Phenom.* **1995**, *73*, 1.
(33) Durmeyer, O.; Kappler, J. P.; Beaurepaire, E.; Heintz, J. M.; Drillon, M. *J. Phys: Condens. Matter* **1990**, *2*, 6127.
(34) Luca, V.; Djajanti, S.; Howe, R. F. *J. Phys Chem. B* **1998**, *102*, 10650.

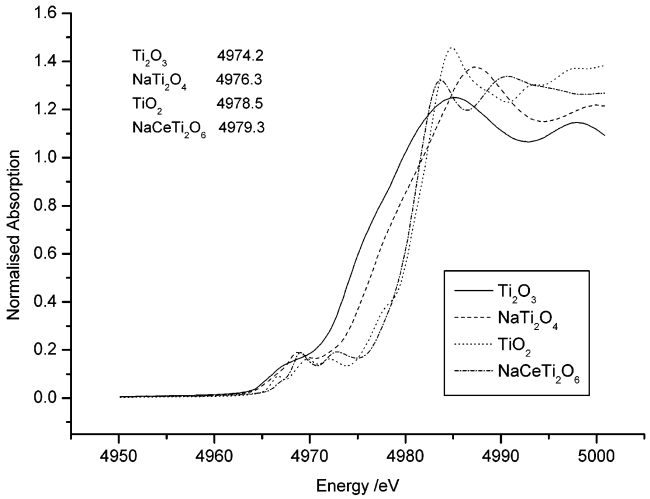

Figure 3. Titanium K-edge XANES data of $NaCeTi_2O_6$ and three crystalline materials containing known oxidation state for titanium: TiO_2 [Ti(IV)], $NaTi_2O_4$ [Ti(3.5)], and Ti_2O_3 [Ti(III)]. Edge positions quoted are the energy at which normalized absorption is 0.5.

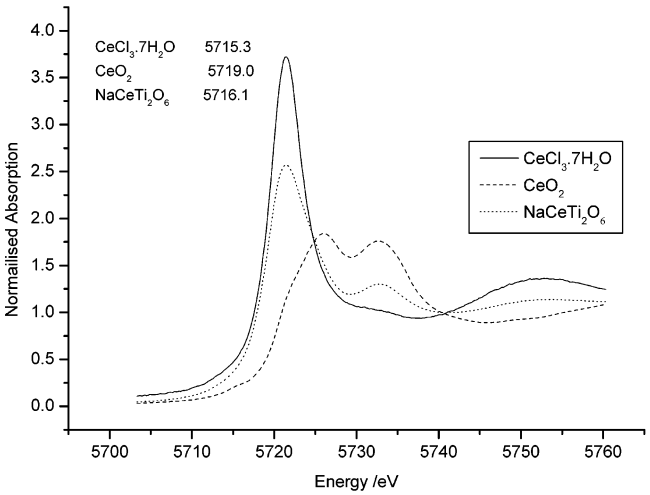

Figure 4. Cerium L_{III}-edge XANES data of $NaCeTi_2O_6$ along with CeO_2 and $CeCl_3 \cdot 7H_2O$. Edge positions quoted are the energy at which normalized absorption is 0.5.

XANES spectrum of $NaCeTi_2O_6$ resembles most closely that of anatase, TiO_2, in terms of both edge position and form of the near-edge structure; thus we conclude that the material contains Ti^{IV} in an octahedral environment. It should be noted that titanium(IV) in other coordination geometries exhibits distinctively different preedge structure in its XANES spectrum.[35,36]

The cerium L_{III}-edge XANES spectrum of $NaCeTi_2O_6$ is shown in Figure 4, along with the data from materials containing solely Ce(III) and Ce(IV). Once again it can be seen that the edge position observed in data from material with the lower oxidation state occurs at a lower energy. Cerium L_{III}-edge XANES data have been used previously to probe the cerium oxidation state, and it is well-established that the near-edge structures of the data are distinctly different for each oxidation state: cerium(IV) exhibits a distinct double peak in the immediate postedge region, and this is true for both oxide and halide materials.[37,38] It should be noted that the intensity of the white line depends strongly upon the precise atomic environment of the element studied. Thus, we can deduce that in $NaCeTi_2O_6$ cerium is found solely in oxidation state +3 from both the edge position and the form of the Ce L_{III} edge.

To understand the formation of $NaCe^{III}Ti^{IV}_2O_6$ from solutions of $Ce^{III}Cl_3$ and $Ti^{III}F_3$, we attempted to investigate the reagent mixture prior to heating in the hydrothermal autoclave. Powder XRD of the solid formed after mixing the reagents for only 30 min at room temperature showed that, remarkably, $NaCeTi_2O_6$ is the sole product. TiF_3 alone is rather unreactive in basic solution at room temperature and may be recovered easily by filtration, and even after hydrothermal treatment at 240 °C, an amount remains, along with a poorly ordered material with a low-angle reflection ($d = 9.82$ Å). The relative stabilities of each oxidation state of the metals are important to consider when preparing cerium titanium oxides. As mentioned in the Introduction, a range of combinations of oxidation states for each metal has been accessed in mixed-metal systems by ceramic routes; for example, Preuss and Gruehn prepared Ce^{3+}/Ti^{4+} mixed oxides by a redox reaction between Ce^{4+} and Ti^{3+} oxides.[18] In our solution-mediated reactions the situation is more complex since we are dealing with heterogeneous reactions in which the insolubility of certain products might have an influence over the outcome of reaction. Also, the reactions are performed at high pH under nonambient pressure and temperature, so standard redox data are not appropriate for predicting the outcome of a reaction. It is perhaps not surprising that the Ti^{3+} in the starting material is oxidized to Ti^{4+} given that the lower oxidation state of titanium is rather reducing; indeed in a previous hydrothermal reaction the Ti^{4+}-containing silicate $K_2TiSi_6O_{15}$ was produced from Ti^{3+} under basic conditions.[39] It is likely that atmospheric oxygen was responsible for the oxidation. In the absence of NaOH, it is interesting to note that CeO_2 and TiO_2 are the only crystalline solid products in our reactions. The driving force for the stabilization of $NaCeTi_2O_6$ is likely to be its rapid precipitation from NaOH solution. If other bases are used, then the Ce^{3+} in solution is oxidized to Ce^{4+} and CeO_2 is produced.

Scanning electron micrographs of hydrothermal $NaCeTi_2O_6$ are shown in Figure 5. The sample is made up of agglomerations of small crystallites (less than 1 μm), but these are not well-formed particles, such as have been seen in hydrothermally prepared $BaTiO_3$ where spherical particles of uniform dimension are often seen.[8] After firing the hydrothermal $NaCeTi_2O_6$ at 1400 °C, despite no change in the powder X-ray diffraction pattern, the electron micrographs reveal that the particle morphology is dramatically altered (Figure 5b), with the sample made up of much larger particles with sharp edges, characteristic of a highly crystalline sample.

(35) Farges, F.; Brown, G. E.; Rehr, J. R. *Geochim. Cosmochim. Acta* **1996**, *60*, 3023.
(36) Mountjoy, G.; Pickup, D. M.; Wallidge, G. W.; Anderson, R.; Cole, J. M.; Newport, R. J.; Smith, M. E. *Chem. Mater.* **1999**, *11*, 1253.
(37) Skanthakumar, S.; Soderholm, L. *Phys. Rev. B* **1996**, *53*, 920.
(38) Takahashi, Y.; Sakami, H.; Nomura, M. *Anal. Chim. Acta* **2002**, *468*, 345.
(39) Zou, X. D.; Dadachov, M. S. *J. Solid State Chem.* **2001**, *156*, 135.

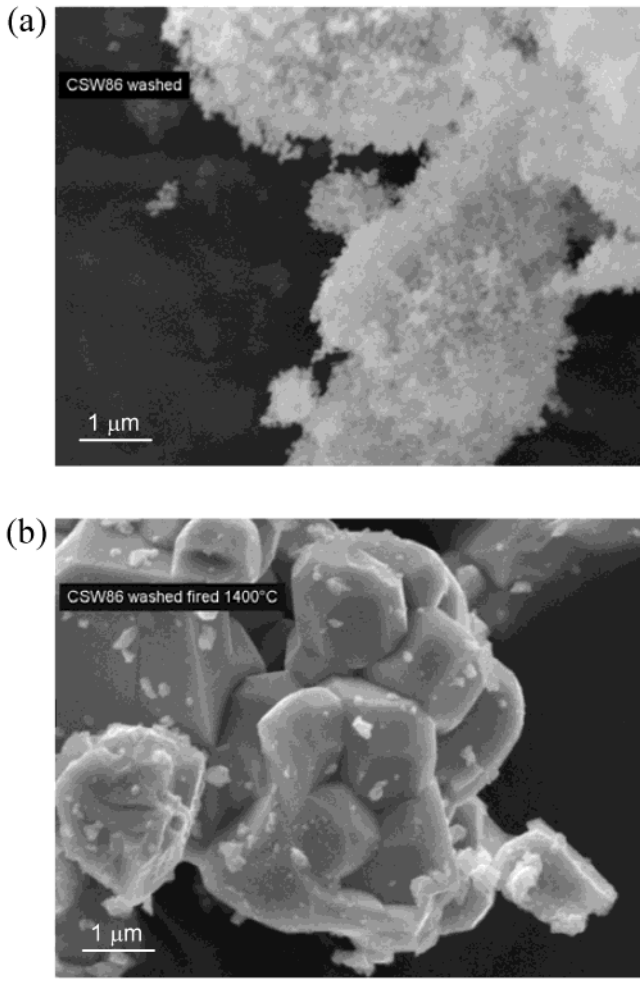

Figure 5. Scanning electron micrographs of (a) hydrothermal $NaCeTi_2O_6$ and (b) $NaCeTi_2O_6$ after firing at 1400 °C in air.

$NaCe_{1-x}Nd_xTi_2O_6$. Since we had proved that cerium exists in oxidation state +3 in synthetic loparite, the incorporation of other trivalent lanthanides into the material was attempted. This proved successful for Nd^{3+}, and pale lilac powders were recovered from the hydrothermal reaction mixture. ICP analysis confirmed the bulk chemical composition of the solids: for example, $NaNdTi_2O_6$: found, 41.1% Nd and 20.2% Ti; expected, 40.2% Nd and 26.7% Ti. Powder X-ray diffraction showed that the materials are isomorphous with $NaCeTi_2O_6$ (orthorhombic, *Pmna*, $a = 5.4628(16)$ Å, $b = 7.7240(30)$ Å, $c = 5.4526(13)$ Å); see Figure 6. Interestingly, the refined unit cell volume of $NaNdTi_2O_6$ (230.07(21) Å^3) is virtually identical to that of $NaCeTi_2O_6$ (230.19(17) Å^3). In other phases where cerium(III) is substituted for by neodymium(III), only a small change in unit cell volume has been reported. For example, in $Nd_{2-x}Ce_xCuO_4$ the cell volume changes by only 1 Å^3 between $x = 0.05$ and $x = 0.3$.[40] The titanium K-edge XANES of $NaNdTi_2O_6$ showed the presence of solely Ti(IV), as found for $NaCeTi_2O_6$.

$NaCeTi_{2-x}V_xO_6$. Figure 6b shows powder X-ray diffraction data measured from $NaCeTiVO_6$. This material was prepared by using a 1:1.25:1.25 ratio of $CeCl_3$, TiF_3, and VCl_3 using hydrothermal synthesis at 240 °C. ICP analysis gave results in agreement with the bulk composition: found, 40.3% Ce, 13.8% Ti, and 12.5% V; expected, 39.5% Ce, 13.3% Ti, and 14.2% V. $NaCeTiVO_6$ is one of a series of materials $NaCeTi_{2-x}V_xO_6$ ($0 \le x \le 1.8$) that can be prepared at 240 °C under hydrothermal conditions, and that are isomorphous with $NaCeTi_2O_6$. The unit cell parameters do not change significantly on substitution of Ti^{IV} by V^{IV}. A search of the ICSD database reveals no simple examples of an isomorphous series with Ti^{IV}/V^{IV} substitution, but if we compare TiO_2[41] and VO_2[42] (both in the rutile modification), the unit cell volume of the former is only 3 Å^3 (5%) larger than the latter. For our system where the occupation of A site of the perovskite structure remains unchanged, we expect an even smaller change in unit cell volume when the Ti^{IV}/V^{IV} substitution is performed, and thus it will be difficult to detect any change in the powder diffraction data. The $NaCeTi_{2-x}V_xO_6$ materials range from pale brown to black in color with increasing substitution of titanium by vanadium. The darker color of the vanadium-substituted materials indicates a delocalization of the V(IV) $3d^1$ electrons, and thus is consistent with our oxidation state assignment. Interestingly, unlike $NaCeTi_2O_6$, these materials are only formed under hydrothermal conditions ($T = 240$ °C): after stirring the reagents at room temperature, the recovered solid is pale yellow and amorphous to X-rays. Attempts to make $NaCeV_2O_6$ by the hydrothermal method were never successful: the product always consisted of CeO_2, $Ce(OH)_3$, and VO_2.

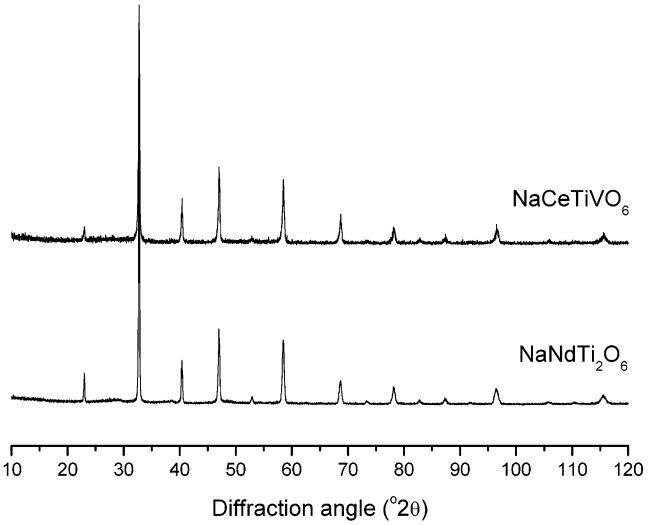

Figure 6. Powder X-ray diffraction data of hydrothermal $NaNdTi_2O_6$ and $NaCeTiVO_6$.

Figure 7 shows the Ti K-edge and V K-edge XANES of $NaCeTiVO_6$ with data measured from the crystalline, model compounds. The Ti K-edge XANES data clearly indicate the presence of titanium(IV) based on analysis similar to that above. The vanadium K-edge XANES indicates that the near-edge structure of the data for $NaCeTiVO_6$ resembles most

(40) Paulus, E. F.; Yehia, I.; Fuess, H.; Rodriguez, J.; Vogt, T.; Stroebel, J.; Klauda, M.; Saemann-Ischenko, G. *Solid State Commun.* **1990**, *73*, 791.

(41) Baur, W. H.; Khan, A. A. *Acta Crystallogr., Sect. C* **1971**, *27*, 2133.
(42) Rogers, K. D. *Powder Diffraction* **1993**, *4*, 240.

Table 2. Parameters Extracted by Gaussian Fitting of the Vanadium K-Edge XANES Spectra

compound	preedge peak center (eV)	edge peak center (eV)	postedge peak center (eV)	area of preedge
VCl_3	5463.8	5473.6	5479.0	0.14
$VO(SO_4)\cdot 5H_2O$	5464.2	5480.1	5492.3	1.3
NH_4VO_3	5464.4	5484.3	5499.9	2.1
$NaCeVTiO_6$	5464.6	5478.2	5487.3	1.1

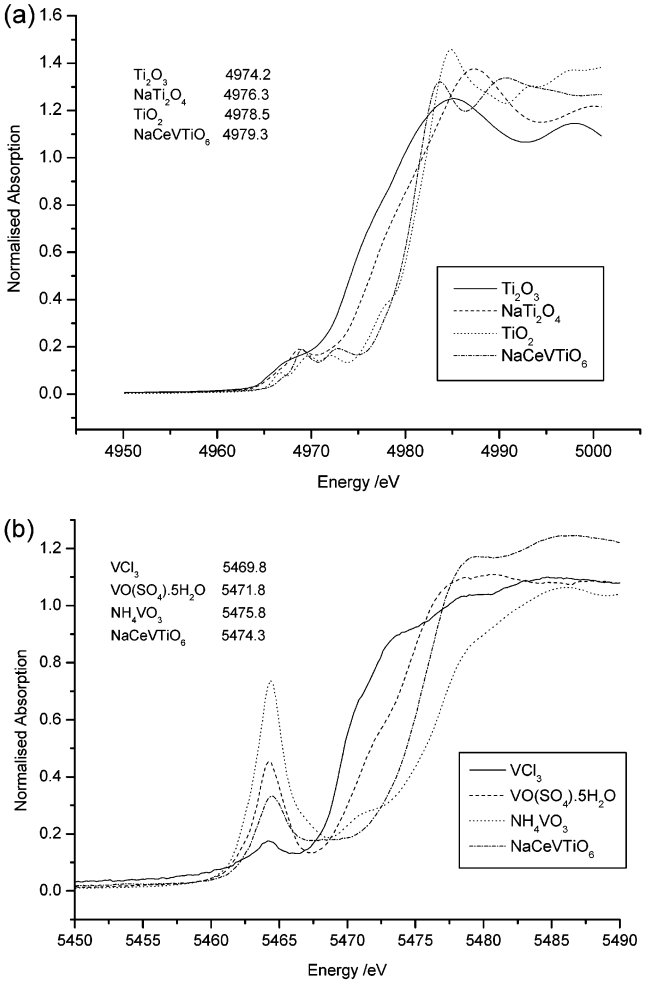

Figure 7. XANES of $NaCeTiVO_6$ with data from crystalline standards: (a) titanium K-edge spectra; (b) vanadium K-edge spectra.

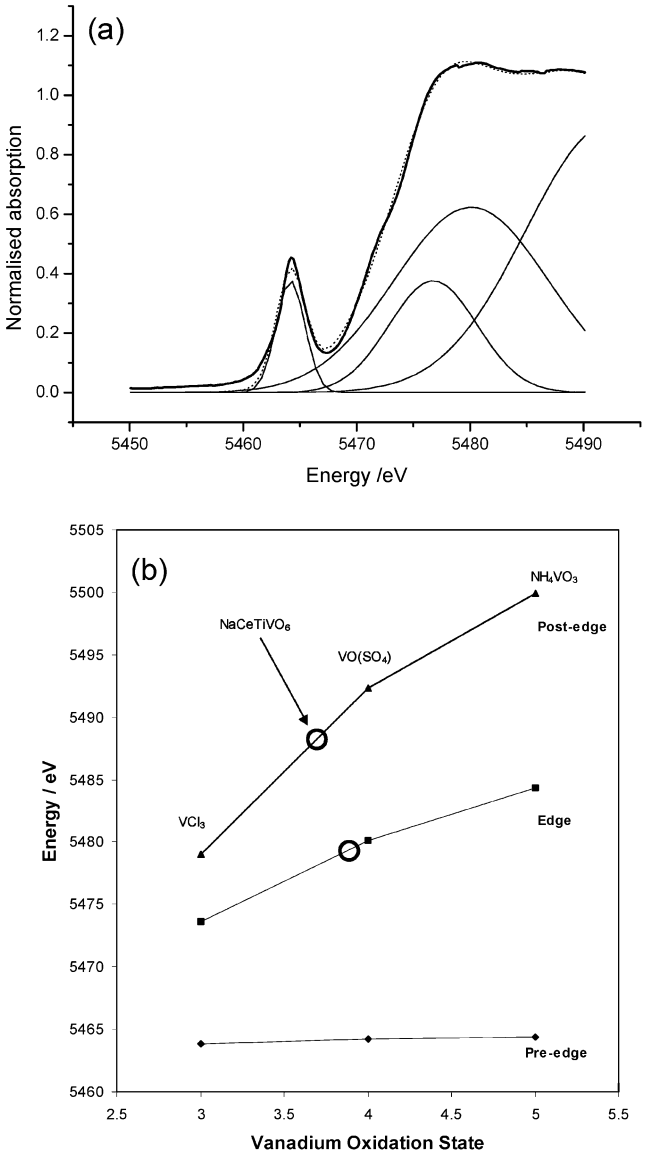

Figure 8. (a) Example of the Gaussian fitting of vanadium K-edge XANES data ($VOSO_4$); (b) plots of energies of fitted Gaussians as a function of vanadium oxidation state.

closely that of the V(IV) model compound, $VO(SO_4)$, but since our vanadium model compounds contain the metal in a variety of coordination geometries, we used several of the spectral features to confirm the oxidation state. The value of energy at normalized absorption of 0.5 is not completely unambiguous in this case, but by using a Gaussian-fitting routine, we can determine the position and relative area of the preedge feature, the edge itself, and also the first postedge feature. The preedge feature is assigned as the 1s−3d transition, and the first strong postedge peak is the 1s−4p dipole-allowed transition.[43] At energies above the latter peak, the XANES data are complex and contain contributions from a variety of processes, including multiple scattering. A typical Gaussian fit is shown in Figure 8a, and the results obtained are contained in Table 2 and also shown graphically in Figure 8b. Such a deconvolution approach to the analysis of XANES data has been previously undertaken, and our results confirm that the vanadium oxidation state affects most strongly the position of the near-edge region, whereas the preedge feature is less affected.[43,44] The data suggest strongly that vanadium is found in oxidation state +4 in $NaCeTiVO_6$: this is consistent with the isomorphous substitution of Ti(IV) and also the dark color of the material due to the presence of the $3d^1$ metal centers. It is tempting to use also the intensity of the preedge feature to deduce the oxidation state of vanadium, and although here for the model compounds we have

(43) Wong, J.; Lytle, F. W.; Messmer, R. P.; Maylotte, D. H. *Phys. Rev. B* **1984**, *30*, 5596.

(44) Nabavi, M.; Taulelle, F.; Sanchez, C.; Verdaguers, M. *J. Phys. Chem. Solids* **1990**, *51*, 1375.

chosen a clear trend of increasing preedge intensity with oxidation state is seen, it is well established that the intensity of this spectral feature also contains information about the local atomic structure about vanadium, and not just oxidation state. This is because the 1s−3d transition is dipole-forbidden, and as the symmetry about vanadium is lowered from octahedral, 3d−4p mixing takes place so that the preedge transition becomes dipole-allowed. Thus, in general, for tetrahedrally coordinated vanadium, as in NH_4VO_3, the intensity of the preedge feature is largest, irrespective of vanadium oxidation state. The cerium L_{III}-edge XANES of $NaCeTiVO_6$ confirms that cerium is present as Ce(III); thus on substitution of titanium by vanadium in $NaCeTi_2O_6$, the oxidation states of all metals are retained.

Conclusions

Hydrothermal reactions between lanthanide salts, titanium trifluoride or TiO_2 (anatase), and transition metal salts in aqueous sodium hydroxide yield highly crystalline mixed-metal oxides related to the mineral loparite and having general formula $NaLnTi_{2-x}M_xO_6$ (Ln = Ce, Nd, M = V). Most of these reactions require the use of hydrothermal conditions (100−240 °C and periods of heating of several hours), but it is noteworthy that $NaCeTi_2O_6$ also forms at room temperature. The use of bases other than sodium hydroxide always results in mixtures of CeO_2 or CeF_3 and TiO_2, and when sodium hydroxide is used, sodium is always incorporated into the perovskite structure. Although this hydrothermal route does not permit the formation of materials in the ternary Ce−Ti−O system, the low-temperature preparation of multinary perovskite oxides provides a very convenient route to these complex solids. It also allows easy access to cerium(III) materials, which is difficult at high temperature in air, since reducing agents are required to prevent oxidation to Ce(IV). Using the ceramic route, it is notoriously difficult to control metal oxidation state, since prolonged heating at extreme temperatures may in some cases actually cause reduction. This is the first report of the $NaCe^{III}Ti^{IV}_{2-x}V^{IV}_xO_6$ series, and we will shortly investigate the magnetic properties of these materials.

Acknowledgment. We thank the EPRSC for funding, Johnson Matthey plc for a CASE studentship for C.S.W., and the CCLRC for provision of beam time at the Daresbury SRS. We are grateful to Dr. Lorrie Murphy for her assistance with running the XAFS experiments, Tony Busby (JM) for the XPS analysis, and Greg Goodlet (JM) for the SEM analysis. We acknowledge the use of the EPSRC Chemical Database Service at Daresbury Laboratory.

Supporting Information Available: Powder XRD data and XPS data. This material is available free of charge via the Internet at http://pubs.acs.org.

IC035211U